RSC Advances

PAPER

View Article Online
View Journal | View Issue

Cite this: *RSC Adv.*, 2017, **7**, 54638

MoS_2 quantum dots featured fluorescent biosensor for multiple detection of cancer†

Yuhong Liu, Jinzha Zhang, Yang Shen, Jinduo Yan, Zaiying Hou, Chun Mao and Wenbo Zhao *

Received 22nd August 2017
Accepted 27th October 2017

DOI: 10.1039/c7ra09300d

rsc.li/rsc-advances

Transition metal ions, such as those generated through MoS_2 material, possess an intrinsic fluorescence quenching property towards organic dye molecules; thus, they can be used to construct biosensors as quenchers. However, we found that the conventional bulk MoS_2 blocks the view of fluorescence imaging, and is incapable of tracing and visualizing mucin 1-overexpression cancer cells. Herein, a FAM fluorophore-labeled ssDNA fluorescent probe (P_0-FAM) stacked on the surface of MoS_2 quantum dots (QDs) was used to construct a MoS_2 QDs–P_0-FAM biosensor. MoS_2 QDs exhibit a high fluorescence quenching ability towards fluorescent dyes, possess large specific surface area and a large number of active sites to adsorb and quench more fluorescent probes, promoting sensitivity between quenching and the recovery signal. In addition, the lighter color of unstack-MoS_2 QDs is beneficial to define the location of cancer cells compared to MoS_2 nanosheets. The novel MoS_2 QDs-based biosensor demonstrates high sensitivity to MUC1 with a detection limit of 0.5 nM, and may become an important tool toward the detection of cancer cells.

Introduction

Breast cancer is, by far, the most frequent cause of cancer deaths in women.[1] For this reason, early detection and early diagnosis are critical factors to guarantee treatability and curability.[2] As studies have reported, MUC1 is a transmembrane glycoprotein, which is abnormally expressed in all stages of development of human adenocarcinomas.[3–5] Overexpression of MUC1 in mammary glandular cells, compared with normal cells, is likely to alter its function and affect the behavior of cancer cells. Therefore, MUC1, as a biomarker indicator, is widely used for early detection of breast cancer.[6,7]

General techniques for detecting MUC1 and cancer cells include flow cytometry, DNA chip technology and PCR techniques; however, these methods usually involve complex instruments and lack efficiency.[8] In addition, the fluorescence method has characteristics of high sensitivity, strong anti-interference and rapid response, as well as tracking and visualizing analytes *via* fluorescence imaging.[9–11] To overcome the drawbacks of time-consumption, high cost and complexity of fluorescent biosensors,[12–14] we require to construct a simple fluorescent biosensor with sensitive signal and strong specificity recognition abilities to detect MUC1 and MCF-7. Recently, transient metal quantum dots were employed as nanoprobes for biological applications due to their fluorescent, paramagnetic properties, radio-opacity, and quenching ability.[15–17] As far as we know, transition metal ions possess an intrinsic fluorescence quenching property towards organic dye molecules.[18] Typically, MoS_2, as an ultrathin direct bandgap semiconductor, has found wide spread applications in optoelectronics, nanoelectronics, and energy harvesting,[19–21] and can act as a fluorescence quencher due to its capacity of quenching dye-labeled single-stranded DNA (ssDNA) *via* van der Waals force or coordination,[22–24] which opens new analytical opportunities.[25] However, fluorescent imaging applications of frequently-used quencher MoS_2 nanosheets remain significantly challenging. The multi-layer stack of MoS_2 nanosheets blocks the view of fluorescence imaging making it hard to clearly observe the location of cancer cells. In this study, we chose MoS_2 QDs to solve this problem.

Herein, we constructed a novel, simple and sensitive MoS_2 QDs-based sensing platform for the assay of MUC1. The biosensor is composed of a fluorescent probe (FAM fluorophore-labeled ssDNA, defined as P_0-FAM) and a quencher (MoS_2 QDs). MoS_2 QDs can recognize complementary oligonucleotides or aptamers as recognition units.[26,27] In addition, they can spontaneously adsorb P_0-FAM *via* van der Waals force between the nucleobases of ssDNA and the surface of MoS_2 QDs. The intrinsic fluorescent quenching property of MoS_2 to organic dye molecules causes fluorescence quenching of P_0-FAM when P_0-FAM is adsorbed on MoS_2 QDs, while the fluorescence recovery of P_0-FAM occurs under the attack of

National and Local Joint Engineering Research Center of Biomedical Functional Materials, Jiangsu Key Laboratory of Biofunctional Materials, School of Chemistry and Materials Science, Nanjing Normal University, Nanjing, 210023, China. E-mail: zhaowenbo@njnu.edu.cn

† Electronic supplementary information (ESI) available. See DOI: 10.1039/c7ra09300d

MUC1, which is attributed to the exposure of P_0-FAM due to the detachment of P_0-FAM from MoS_2 QDs with a stronger affinity between P_0-FAM and MUC1.[28–31] The employment of MoS_2 QDs is beneficial in fluorescence imaging to detect the location, the size of the tumor and the treatment region due to larger specific surface area, more active sites to adsorb more fluorescent probes, and the lighter color of unstack-MoS_2 QDs compared to MoS_2 nanosheets. The MoS_2 QDs–P_0-FAM-based fluorescent biosensor with sensitive signal and strong specificity recognition abilities to MUC1 is expected to provide a new perspective for the detection and diagnosis of breast cancer.

Materials and reagents

Molybdenum(IV) sulfide (99%) was supplied by Energy Chemical. Ethanol absolute, sodium chloride, sodium dihydrogen phosphate, dehydrate, disodium phosphate dibasic dodecahydrate and potassium chloride were all supplied by Sinopharm Chemical Reagent Co. Ltd. Thiazolyl blue tetrazolium bromide (MTT) was obtained from Aladdin Industrial Co. Ltd. Dulbecco's modified Eagle's medium (DMEM)/high glucose, trypsin–EDTA solution, fetal bovine serum, phosphate buffer solution (NaCl 136.89 mM, KCl 2.67 mM, Na_2HPO_4 10.15 mM, KH_2PO_4 1.76 mM, pH 7.2–7.4), penicillin–streptomycin solution (100×) and P_0-FAM (5′ to 3′: GCAGTTGATCCTTTGGAT-ACCCTGG, 5′ decorated with FAM fluorophore) were purchased from Sangon Biotech Co. Ltd. (Shanghai, China). Porcine bone marrow mesenchymal stem cells (PBMSC) were provided by Nanjing Gulou Hospital. Human mammary carcinoma (MCF-7) cells and mouse fibroblast cells (L929) were purchased from Shanghai Cell Bank. All the chemicals were of analytical grade and used without further purification.

MUC1 (N → C: PDTRPAPGSTAPPAHGVTSAPDTRPAPG-STAPPAHGVTSA) was obtained from China Peptides Co. Ltd. (Shanghai, China).

Instrumentation

A draught drying cabinet, numerical control ultrasonic cleaners and a medical centrifuge were used to prepare the MoS_2 QDs. Transmission electron micrograph (TEM) was obtained using an H-7650 TEM instrument (Hitachi, Japan). The X-ray diffraction (XRD) pattern was recorded on a D/max 2005VL/PC X-ray diffractometer (Rigaku, Germany). X-ray photoelectron spectroscopy (XPS) was conducted with PHI Quantera II. Zeta potential analysis was performed on a dynamic light scatter (DLS, NANO-ZS920, Malvern, UK). Fluorescence spectra were recorded on an F-4600 spectrofluorometer (HITACHI, Japan) equipped with a xenon lamp, $\lambda_{ex} = 490$ nm, $\lambda_{em} = 520$ nm. The PMT voltage was 620 V and the slits for both the excitation and the emission were set at 10 nm. The MTT assay was obtained using a Varioskan flash microplate reader (Thermo Scientific) at 490 nm. The confocal microscopy experiments were conducted using a MRC-1024 (Bio-Rad, Ltd., USA).

Synthesis of water-soluble MoS_2 QDs

MoS_2 QDs were prepared by a modified mixed solvent strategy for liquid exfoliation.[32] Initially, 60 mg MoS_2 powder was mixed with 20 mL of ethanol/water with an ethanol volume fraction of 45% in a 50 mL flask. The sealed flask with the mixture was ultrasonicated for 24 h and a dark green suspension was obtained. The dispersion was centrifuged at 2000 rpm for 10 min three times to remove the aggregates. Following this, the supernatant was centrifuged at 10 000 rpm for 10 min and collected at 60 °C in a drying cabinet to remove the ethanol and water absolutely. Next, the product was dissolved in deionized water and centrifuged at 2000 rpm for 10 min to remove the larger MoS_2 nanoparticles. Finally, the supernatant was filtered through a 0.22 μm Millipore membrane filter and collected at 60 °C in a drying cabinet.

Selection of MoS_2 QDs concentration and kinetic assay

The MoS_2 QDs solution was diluted by PBS buffer (pH 7.4) to a final concentration of 500 μg mL^{-1}. Different volumes (0–200 μL) of MoS_2 QDs solution (500 μg mL^{-1}) were mixed with 100 μL of 100 nM P_0-FAM in a 2.0 mL centrifugal tube; different volumes of PBS buffer were added to make 500 μL of each solution. The final P_0-FAM concentration was 20 nM, and the concentrations of MoS_2 QDs were 0, 5, 10, 15, 20, 30, 50, 100, and 200 μg mL^{-1}. Then, these mixtures were allowed to react for 30 min at 37 °C. Finally, fluorescence measurements were performed at room temperature.

Kinetic assay was performed on the fluorescence quenching and fluorescence recovery. For fluorescence quenching, 100 μL of MoS_2 QDs solution (500 μg mL^{-1}) was mixed with 100 μL of 100 nM P_0-FAM in a cuvette. The fluorescence measurements were performed at different times (0–6 min) at room temperature. For fluorescence recovery, 100 μL of MoS_2 QDs solution (500 μg mL^{-1}) was mixed with 100 μL of 100 nM P_0-FAM in the cuvette; after 15 min at room temperature, 250 μL MUC1 and 50 μL PBS were added into the reaction mixture. The fluorescence measurements were performed at different times (0–10 min) at room temperature.

Assay for MUC1 in aqueous buffer

100 μL of MoS_2 QDs solution (500 μg mL^{-1}) was mixed with 100 μL of 100 nM P_0-FAM in a test tube; then, the mixed solution was allowed to react for 6 min at room temperature. Following this, different volumes of MUC1 (20 μM) in PBS buffer (0–250 μL) were added. Finally, different volumes of PBS buffer (pH 7.4) were introduced to prepare 500 μL of each reaction solution and the final MUC1 concentration (0, 0.001, 0.005, 0.010, 0.050, 0.100, 0.500, 2, 3, 4, 5, 6, 7, 8, 9, and 10 μM). The final mixed solution was allowed to react for 10 min at 37 °C. The fluorescence spectra were measured at room temperature.

Cell culture and MTT experiments

MCF-7 cells, PBMSC and L929 cells were cultured in a cell culture flask in Dulbecco's modified Eagle's medium (DMEM)/high glucose containing 10% fetal bovine serum (FBS) and 1% penicillin–streptomycin solution (100×) at 37 °C under an incubator containing 5% CO_2.

MCF-7 was incubated with different concentrations of MoS_2 QDs (10–200 μg mL^{-1}) at 37 °C and in 5% CO_2 for 24 h. Further,

the cell viability experiments were conducted using a Varioskan flash microplate reader (Thermo Scientific) at 490 nm. The cell viability was then assessed using the equation below:

$$\text{Cell viability } (\%) = \frac{\text{OD value of treatment group}}{\text{OD value of control group}} \times 100\%$$

Assay for MCF-7 cells in DMEM

Initially, 1 mL of MoS_2 QDs solution (500 μg mL^{-1}) was mixed with 1 mL of 100 nM P_0-FAM in a test tube; the mixed solution was allowed to react for 6 min at room temperature. Then, 200 μL of the mixed solution was added to different concentrations of MCF-7 (0 to 5 × 10^5 cells per mL). After incubation at 37 °C for 30 min, the fluorescence spectra were measured at room temperature.

Selectivity assays

The selectivity assays were tested by comparing the fluorescence signal changes of samples containing glucose oxidase (GOD), cytochrome c (CyC), myoglobin (Mb), Lys and bovine serum albumin (BSA). Initially, 1 mL of MoS_2 QDs solution (500 μg mL^{-1}) was mixed with 1 mL of P_0-FAM (100 nM) in a test tube; the mixed solution was allowed to react for 10 min at room temperature. Then, 200 μL of the mixed solution was added to the sensing systems containing 10 μM MUC1, 100 μM glucose oxidase (GOD), 100 μM cytochrome c (CyC), 100 μM myoglobin (Mb), 100 μM Lys and 100 μM bovine serum albumin (BSA). After incubation at 37 °C for 15 min, the fluorescence spectra were measured at room temperature.

Results and discussion

Characterization of MoS_2 QDs

The morphology of MoS_2 was studied using TEM (Fig. 1). The synthetic MoS_2 QDs (Fig. 1B and C) are dispersed evenly in aqueous solution compared to MoS_2 nanosheets in aqueous solution (Fig. 1A). TEM images revealed that the average size of smaller MoS_2 QDs, which were used for further experiments, were about 3 nm (Fig. 1C and D). The XRD patterns (Fig. 2A) of the samples matched well with that of 2H-MoS_2 (JCPDS: 24-513). As can be observed, the primary diffraction peaks at 14.4°, 33.2° and 58.4° were attributed to the (002), (100) and (110) planes of the hexagonal MoS_2, respectively, indicating the high purity of the obtained smaller MoS_2 QDs.[33] Raman spectrum was used to further confirm that smaller MoS_2 QDs were obtained (Fig. 2B). The Raman spectrum of bulk MoS_2 was well-known with two

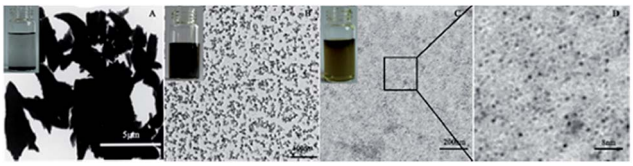

Fig. 1 TEM pictures of MoS_2 (A) nanosheets, (B) large size (QDs), (C) small size (QDs), and (D) the enlarged view of (C).

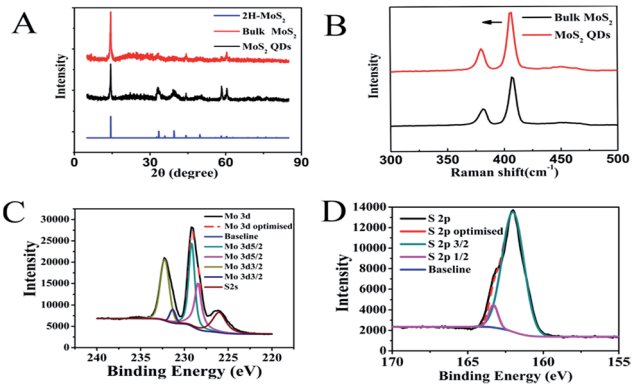

Fig. 2 (A) XRD pattern of MoS_2 QDs. (B) Raman spectra of MoS_2 QDs. XPS survey of (C) Mo atom and (D) S atom in as-prepared MoS_2 QDs.

main modes, the A_{1g} and E_{2g}, corresponding to the out-plane vibrations and in-plane vibrations as located at 408 and 382 cm^{-1}, respectively.[34] This was represented by the black line shown in Fig. 2B. It could be observed that the A_{1g} mode of MoS_2 QDs slightly blue shifted to 405.5 cm^{-1}, which proved that we had successfully prepared MoS_2 QDs.[35] As shown in Fig. 2C, Mo $3d_{3/2}$ and Mo $3d_{5/2}$ peaks could be observed at 232.2 eV and 231.4 eV and 229.1 eV and 228.5 eV, respectively. The S 2p peaks at the binding energies of 162.0 and 163.3 eV arise from S $2p_{3/2}$ and S $2p_{1/2}$, respectively (Fig. 2D). The XPS spectra were consistent with those in previously reported literatures, indicating the dominant 2H MoS_2 phase in the MoS_2 QDs.[36,37] The zeta potential of the MoS_2 QDs were determined to be −27.8 mV (Fig. S1†), suggesting the great colloidal stability of the MoS_2 QDs in aqueous media.

Mechanism of the fluorescent biosensor

Scheme 1 displays the principle diagram of the DNA biosensor composed of the quencher (MoS_2 QDs) and the fluorescent probe (P_0-FAM). The fluorescence quenching of P_0-FAM occurred when MoS_2 QDs adsorbed P_0-FAM *via* the van der Waals force between the nucleobases of ssDNA and the surface of MoS_2 QDs owing to the possible transfer of

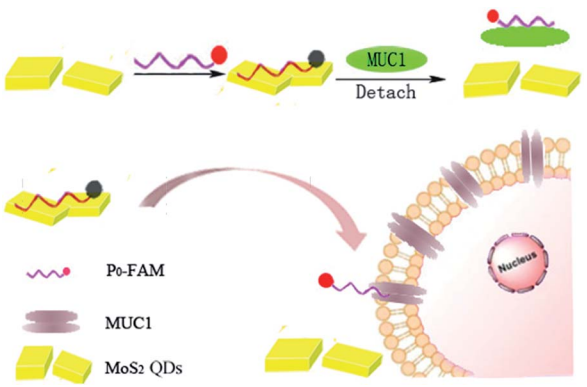

Scheme 1 Preparation procedures of probe for MUC1 and MCF-7 detection based on FL signal.

electrons or energy between the closely connected dye molecules and the MoS_2 QDs (Fig. S2†). Interestingly, in the presence of MUC1, the fluorescence recovery of P_0-FAM could be observed because MoS_2–P_0-FAM adopted a rigid and definite tertiary structure owing to the specific binding between ssDNA and MUC1. The affinity of ssDNA with MUC1 was stronger than that of MoS_2 QDs, resulting in the release of the P_0-FAM from the QDs surface and recovery of the fluorescence signal. In contrast, without MoS_2 QDs, P_0-FAM was primarily in the unfolded and flexible state in the presence of MUC1. The FL signal did not drastically change, indicating that MoS_2 QDs as a quencher played a crucial role in turn-on FL biosensor for the sensitive detection of MUC1 in cancer cells.

Optimization of detection conditions

To evaluate the fluorescence-quenching ability of MoS_2 QDs toward P_0-FAM, the fluorescence signal changes were recorded upon mixing P_0-FAM and the prepared MoS_2 QDs. As shown in Fig. 3A, the quenching of FAM fluorescence by MoS_2 depended on the concentration of the quenchers. In the presence of 100 μg mL^{-1} MoS_2 QDs, the emission of the FAM was almost quenched with 90% quenching efficiency (Fig. 3B), revealing a high quenching efficiency of MoS_2 QDs toward the aptamer biosensor. The observed background fluorescence, as shown in Fig. 3B, corresponding to the fluorescence of 200 μg mL^{-1} MoS_2 QDs, could be attributed to the existence of the secondary structure of P_0-FAM at the detection conditions. Fig. 4A and B show the adsorption kinetics of the dye-labeled aptamer biosensor on the MoS_2 QDs. The quenching was rapid and achieved equilibrium in about 4 min. This suggested that the interaction of P_0-FAM with MoS_2 QDs was quite strong and the MoS_2 QDs possessed a high fluorescence-quenching ability. The MoS_2 QDs exhibited robust quenching efficiency possibly because of the better water dispersivity. Furthermore, the fluorescence recovery kinetics was performed and the best fluorescence recovery efficiency was obtained within 8 min when MUC1 was added into the mixture solution (Fig. 4C and D). This suggested that the designed MUC1 biosensor system works successfully and can deliver high performance. In order to achieve more effective detection, 15 min was chosen as the optimal reaction time.

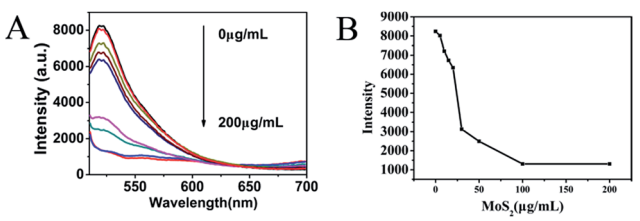

Fig. 3 Fluorescence intensity (A) and trend chart (B) of P_0-FAM (20 nM) after addition of MoS_2 QDs with different concentrations in PBS buffer.

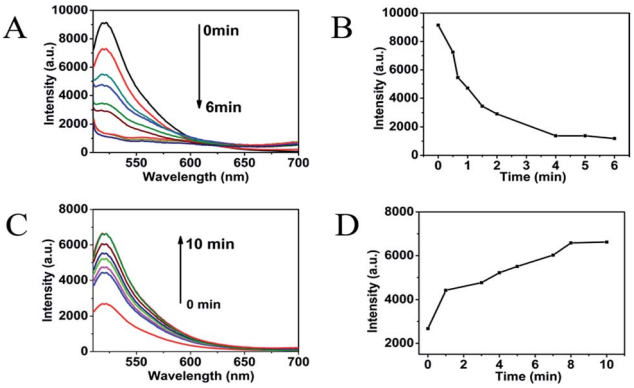

Fig. 4 (A and B) Fluorescence quenching of P_0-FAM (20 nM) in PBS buffer by MoS_2 QDs (100 μg mL^{-1}) as a function of time. (C and D) Optimization of incubation time of P_0-FAM and MUC1. The concentrations of P_0-FAM, MoS_2 QDs were 20 nM and 100 μg mL^{-1}, respectively.

Quantitative analysis of MUC1 in aqueous buffer

As shown in Fig. 5, a new simple and sensitive assay for MUC1 was successfully designed. The fluorescence intensity depended on the concentration of MUC1 over a range of 0–10 μM when the concentration of MoS_2 QDs was 100 μg mL^{-1} (Fig. 5A and B). As shown in Fig. 5C, the fluorescence intensity increases rapidly as the concentration of MUC1 increases from 0 μM to 0.5 μM (R^2 = 0.9978). However, it exhibited another linear relationship as shown in Fig. 5D (R^2 = 0.997) when the concentration of MUC1 changed from 0.5 μM to 10 μM, where the fluorescence intensity increased more slowly with the increase in MUC1 concentration. The reason for this phenomenon was probably that P_0-FAM in the state of random coil single strand was correspondingly abundant when MUC1 was less than 0.5 μM in the system, and MoS_2 QDs could strongly adsorb these random coil single-strands FAM-ssDNA onto its surface owing to the weak

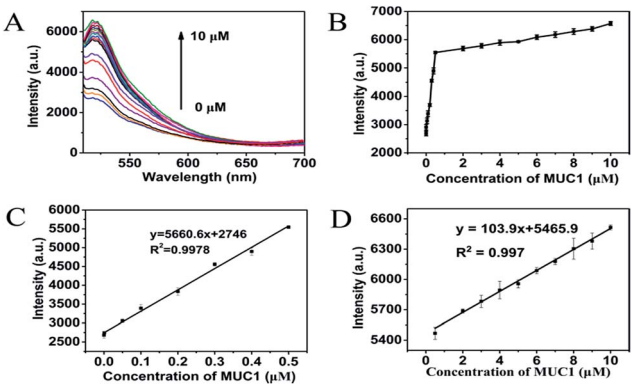

Fig. 5 (A) Fluorescence spectra upon addition of MUC1 with different concentrations. The MUC1 concentrations were 1 nM, 5 nM……8 μM, 9 μM and 10 μM. (B) The relationship between fluorescence intensity at 520 nm *versus* MUC1 concentrations. (C) Linear region at MUC1 concentrations (0.0–0.5 μM). (D) Linear region at MUC1 concentrations (0.5–10 μM). Error bars were estimated from three replicate measurements.

adsorption competition among the free FAM-ssDNA. When MUC1 exceeded 0.5 μM in the system, free FAM-ssDNA in the state of random coil single strand became scarce. The adsorption competition among them became more intense, so the fluorescence intensity changed more slowly as the MUC1 concentration increased. This method could be applied to detect MUC1 concentrations as low as 0.5 nM (3 times the standard deviation rule) in aqueous buffer. Moreover, the detection range was wide, ranging from 0 μM to 10 μM. Combined with the data listed in Table S1,† the results demonstrated that the fluorescent detection of biosensor for MUC1 was feasible for a relatively broad detection range and low detection limit. From this perspective, the proposed method towards MUC1 detection had its own uniqueness, that is, the present method was much simpler and more effective to detect MUC1.

Performance of MCF-7 detection and selectivity assays of FL biosensor

The MTT assays of cell viability studies suggested that MoS_2 QDs did not impose a considerable toxicity towards MCF-7 cells as compared to the control (Fig. 6A). The above results indicated that the as-prepared MoS_2 QDs could be promising biosensors in cell detection and imaging. As shown in Fig. 6B, the fluorescence intensity was dependent on the concentration of MCF-7 cells over a range of 0 to 5×10^5 cells per mL, when the concentration of MoS_2 QDs was 100 μg mL^{-1}. As illustrated in Fig. 6C, a linear relationship between peak intensity at 520 nm and MCF-7 cells concentrations was obtained in the concentration range from 10^3 to 5×10^5 cells per mL ($R^2 = 0.9949$) with a detection limit of 50 cells per mL (according to the rule of three times the standard deviation corresponding to the blank sample detection). Due to the specific binding between P_0-FAM and MUC1, the MoS_2 QDs-based biosensor was insensitive to the interfering proteins such as GOD, CyC, Mb, Lys and BSA as shown in Fig. S3.† The good selectivity, biocompatibility and the intrinsic optical properties of the biosensor can be used to construct an excellent bioimaging system and recognition system.

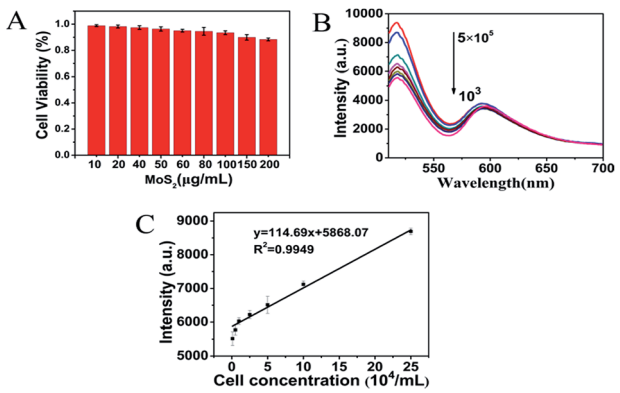

Fig. 6 (A) Viability of MCF-7 cells incubated with different concentration of MoS_2 QDs. (B) Fluorescence spectra upon addition of MCF-7 cells with different concentrations. (C) Linear region at low concentrations of MCF-7 cells.

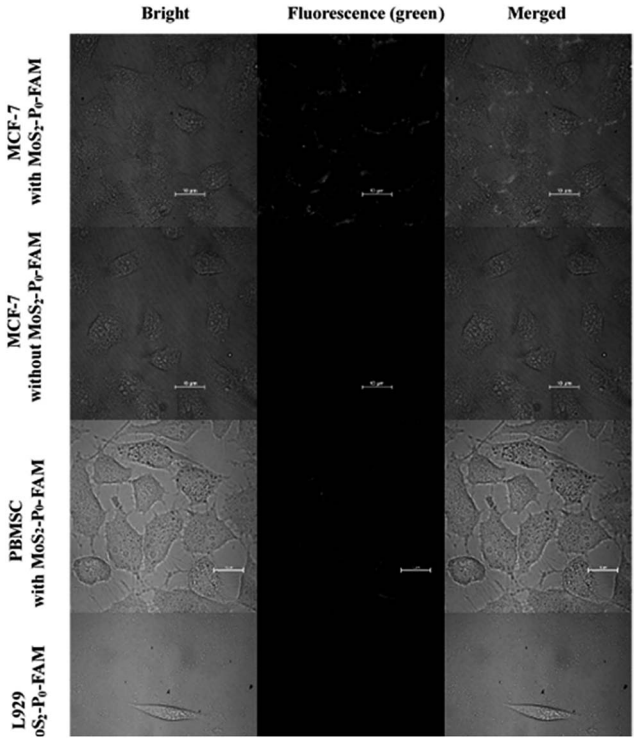

Fig. 7 Confocal fluorescence microphotograph of different cells incubated with MoS_2 QDs featured fluorescent biosensor for 1 h. Scale: 10 μm.

Intracellular imaging analysis

Fluorescence microscope images of MCF-7 cells loaded with the MoS_2–P_0-FAM (MoS_2 QDs) biosensor for 1 h at 37 °C showed green fluorescence on cytomembrane (Fig. 7). However, the control experiment on cells without the MoS_2–P_0-FAM biosensor gave no green fluorescence in the same exposure condition. These results demonstrated the specific recognition of MoS_2–P_0-FAM biosensor to MUC1 in MCF-7 cells. In contrast, the fluorescence for PBMSC and L929 cells exhibited no green fluorescence due to non-overexpression of MUC1 in PBMSC and L929 cells, proving that the MoS_2 QDs-based biosensor can be applied to bioimaging and recognition of MCF-7. By comparison, MCF-7 cells incubated with the MoS_2 sheets–P_0-FAM biosensor showed extremely weak green fluorescence (Fig. S4†), indicating that the multi-layer stacking of MoS_2 nanosheets would block the view of fluorescence imaging and affect the detection of cancer cells. Hence, the MoS_2 QDs-based biosensor was superior to that of MoS_2 sheets.

Conclusion

In summary, this study presented a sensitive MoS_2 QDs based fluorescent sensing platform for MUC1. In particular, we applied MoS_2 QDs to MCF-7 detection and cellular imaging, which is extremely rare in the application of MoS_2. MoS_2 QDs exhibited a high fluorescence quenching ability towards fluorescent dyes; therefore, they were exploited as carrier and quencher for a fluorescent dye-labeled DNA aptamer (P_0-FAM)

to construct a biosensor. The obtained results showed that the detection range of MUC1 in the solution was in the range of 1 nM to 10 μM and the detection limit was 0.5 nM. The detection range of MCF-7 was in the range of 10^3 to 5×10^5 cells per mL and the detection limit was 50 cells per mL. The biosensor also had the advantages of high sensitivity and specificity. Furthermore, we expect that this strategy based on MoS_2 QDs as a fluorescent quencher may offer a new approach in the sensitive and selective detection of a wide spectrum of analytes and cancer cells.

Conflicts of interest

There are no conflicts to declare.

Acknowledgements

This work was supported by the National Natural Science Foundation of China (21571104), Major projects of Natural Sciences of University in Jiangsu Province of China (14KJA150006), Projects of Jiangsu Collaborative Innovation Center of Biomedical Functional Materials, and the Priority Academic Program Development of Jiangsu Higher Education Institution.

Notes and references

1 Y. Li, Y. Zhang, M. Zhao, Q. Zhou, L. Wang, H. Wang, X. Wang and L. Zhan, *Chem. Commun.*, 2016, **52**, 3959–3961.
2 R. Beatson, V. Tajadura-Ortega, D. Achkova, G. Picco, T. D. Tsourouktsoglou, S. Klausing, M. Hillier, J. Maher, T. Noll, P. R. Crocker, J. Taylor-Papadimitriou and J. M. Burchell, *Nat. Immunol.*, 2016, **17**, 1273–1281.
3 Y. He, Y. Lin, H. W. Tang and D. W. Pang, *Nanoscale*, 2012, **4**, 2054–2059.
4 M. Hiraki, T. Maeda, A. Bouillez, M. Alam, A. Tagde, K. Hinohara, Y. Suzuki, T. Markert, M. Miyo, K. Komura, R. Ahmad, H. Rajabi and D. Kufe, *Oncogene*, 2017, **36**, 2791–2801.
5 A. Lui and J. Lewis-Wambi, *Cancer Res.*, 2016, **76**, 2918.
6 X. Y. Jiang, H. J. Wang, H. J. Wang, R. Yuan and Y. Q. Chai, *Anal. Chem.*, 2016, **88**, 9243–9250.
7 A. K. H. Cheng, H. Su, A. Wang and H. Z. Yu, *Anal. Chem.*, 2009, **81**, 6130–6139.
8 W. Ma, W. Zheng, D. Cui, Y. Song and Q. Wu, *Acta Biochim. Biophys. Sin.*, 2000, **32**, 285–289.
9 E. Climent, M. D. Marcos and K. Rurack, *Angew. Chem., Int. Ed.*, 2013, **52**, 8938–8942.
10 C. L. Zhu, C. H. Lu, X. Y. Song, H. H. Yang and X. R. Wang, *J. Am. Chem. Soc.*, 2011, **133**, 1278–1281.
11 K. Cherukula, K. M. Lekshmi, S. Uthaman, K. Cho, C. S. Cho and I. K. Park, *Nanomaterials*, 2016, **6**, 76.
12 P. Wu, X. D. Hou, J. J. Xu and H. Y. Chen, *Nanoscale*, 2016, **8**, 8427–8442.
13 Q. Wu, M. Q. Chu, Y. X. Shao, F. J. Wo and D. L. Shi, *Carbon*, 2016, **108**, 21–37.
14 A. Rammohan, G. Mishra, B. Mahaling, L. Tayal, A. Mukhopadhyay, S. Gambhir, A. Sharma and S. Sivakumar, *ACS Appl. Mater. Interfaces*, 2016, **8**, 350–362.
15 S. Santra, H. Yang, P. H. Holloway, J. T. Stanley and R. A. Mericle, *J. Am. Chem. Soc.*, 2005, **127**, 1656–1657.
16 H. M. Fan, M. Olivo, B. Shuter, J. B. Yi and R. Bhuvaneswari, *J. Am. Chem. Soc.*, 2010, **132**, 14803–14811.
17 G. W. Walker, V. C. Sundar, C. M. Rudzinski, A. W. Wun and M. G. Bawendi, *Appl. Phys. Lett.*, 2003, **83**, 3555–3557.
18 Y. Huang, Y. Shi, H. Y. Yang and Y. Ai, *Nanoscale*, 2015, **7**, 2245–2249.
19 B. Radisavljevic, A. Radenovic, J. Brivio, V. Giacometti and A. Kis, *Nat. Nanotechnol.*, 2011, **6**, 147.
20 K. F. Mak, C. Lee, J. Hone, J. Shan and T. F. Heinz, *Phys. Rev. Lett.*, 2010, **105**, 136805.
21 H. Li, Z. Y. Yin, Q. Y. He, X. Huang, G. Lu, D. W. H. Fam, A. I. Y. Tok, Q. Zhang and H. Zhang, *Small*, 2012, **8**, 63.
22 D. Jariwala, V. K. Sangwan, L. J. Lauhon, T. J. Marks and M. C. Hersam, *ACS Nano*, 2014, **8**, 1102–1120.
23 Y. Shi, W. Zhou, A. Y. Lu, W. Fang, Y. H. Lee, A. L. Hsu, S. M. Kim, K. K. Kim, H. Y. Yang, L. J. Li, J. C. Idrobo and J. Kong, *Nano Lett.*, 2012, **12**, 2784–2791.
24 N. Goswami, A. Giri and S. K. Pal, *Langmuir*, 2013, **29**, 11471–11478.
25 H. Deng, X. Yang and Z. Gao, *Analyst*, 2015, **140**, 3210–3215.
26 L. Mo, J. Li, Q. Liu, L. Qiu and W. Tan, *Biosens. Bioelectron.*, 2017, **89**, 201–211.
27 B. L. Li, J. Wang, H. L. Zou, S. Garaj, C. T. Lim, J. Xie, N. B. Li and D. T. Leong, *Adv. Funct. Mater.*, 2016, **26**, 7034–7056.
28 X. Q. Liu, R. Aizen, R. Freeman, O. Yehezkeli and I. Willner, *ACS Nano*, 2012, **6**, 3553–3563.
29 J. Yang, B. Dou, R. Yuan and Y. Xiang, *Anal. Chem.*, 2016, **88**, 8218–8223.
30 X. Q. Liu, F. Wang, R. Aizen, O. Yehezkeli and I. Willner, *J. Am. Chem. Soc.*, 2013, **135**, 11832–11839.
31 X. Zhang, Z. C. Lai, C. L. Tan and H. Zhang, *Angew. Chem., Int. Ed.*, 2016, **55**, 8816–8838.
32 K. G. Zhou, N. N. Mao, H. X. Wang, Y. Peng and H. L. Zhang, *Angew. Chem., Int. Ed.*, 2011, **50**, 10839–10842.
33 F. E. Wickman and D. K. Smith, *Am. Mineral.*, 1970, **55**, 1843–1856.
34 D. Gopalakrishnan, D. Damien and M. M. Shaijumon, *ACS Nano*, 2014, **8**, 5297–5303.
35 S. Xu, D. Li and P. Wu, *Adv. Funct. Mater.*, 2015, **25**, 1127–1136.
36 W. Dai, H. Dong, B. Fugetsu, Y. Cao, H. Lu, X. Ma and X. Zhang, *Small*, 2015, **11**, 4158–4164.
37 W. Gu, Y. Yan, C. Zhang, C. Ding and Y. Xian, *ACS Appl. Mater. Interfaces*, 2016, **8**, 11272.